

LOS ALAMOS NATIONAL LABORATORY
ACTINIDE RESEARCH
QUARTERLY
3rd Quarter 2007

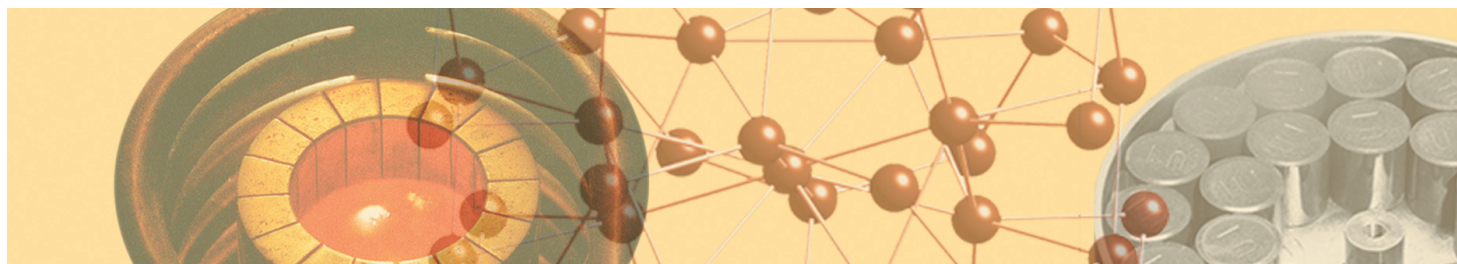
Seaborg Institute Postdocs



CONTENTS

Seaborg Institute Postdoctoral Fellows Program

- Fostering excellence and external visibility in actinide science 1 •
- Theoretical studies of bond-activation chemistry 2 •
- The effects of rhenium doping on the temperature-versus-high magnetic field phase diagram of URu_2Si_2 5 •
- Chain-of-states atomistic calculations of the pathways and energetics of structural phase transformations in plutonium 11 •
- Quantum chemistry approaches to actinide electronic structure 14 •
- Radiation damage effects in uranium-bearing delta-phase oxides 16 •
- Probing the nature of uranium-ligand multiple bonds 18 •
- Shape memory effect deformation structures in a uranium-niobium alloy 20 •
- An investigation of the reactivity of a *trans*-bis(imido) uranium(VI) complex 24 •
- Structure and bonding in actinide complexes 27 •



SEABORG INSTITUTE POSTDOCTORAL FELLOWS PROGRAM

FOSTERING EXCELLENCE AND EXTERNAL VISIBILITY IN ACTINIDE SCIENCE

The primary mission of Los Alamos National Laboratory is national security. Although nuclear weapons are a central focus of the Lab's mission, it is clear that this role is in decline as the threat of a strategic nuclear exchange fades. At the same time, new threats outside the nation's traditional response structure are emerging that are so complex that the state of applied science is inadequate to address them.

Two of these linked threats are the inability of the United States to meet its energy requirements without massive importation of oil and the destructive increase in average global temperature as fossil-fuel-generated carbon dioxide emissions block re-radiation of heat to space. Collateral damage from these two threats include degradation of our economy as U.S. dollars leave in massive amounts, decrease in our ability to invest in science and education as our available resources are spent more and more on energy, and a general decline in the value of the United States to the rest of the world as we import more and export less science and technology. If Los Alamos is to protect national security in the future, it must do so using, among many capabilities, its nuclear expertise, still unchallenged and nationally recognized.

Knowledge of actinide science, including national defense, environmental restoration, radioactive waste management, and especially energy security, continues to be essential to the United States and central to the mission of the National Nuclear Security Administration. As energy security becomes increasingly tied to nuclear power, knowledge and expertise in the production, processing, purification, characterization, analysis, and disposal of actinide elements are essential to national security.

The Seaborg Institute Postdoctoral Fellows Program fosters sustained excellence and enhanced external visibility in actinide science. The program also provides a broad intellectual community for actinide science in support of Laboratory missions as well as a mechanism to attract and retain a future generation of actinide scientists and engineers. Seaborg postdocs perform research that supports new actinide science at the single-investigator or small-team level in the areas of actinide physics, chemistry, metallurgy, sample production, experimental technique development, theory, and modeling.

The Seaborg Postdoctoral Program now supports a dozen or so actinide investigators. With support from the Laboratory Directed Research and Development (LDRD) Program, the Seaborg Institute and its programs, workshops, and seminars provide the focus for communicating and coordinating actinide research at Los Alamos.

Aligning with currently funded and anticipated new actinide-related proposals, the Seaborg Institute provides clear direction to outstanding scientists. It also demonstrates that actinide physics, chemistry, materials science, and engineering remain a high priority and that Los Alamos provides the finest actinide environment in the world. At present, Seaborg postdocs support directly or indirectly LDRD Directed Research programs in several divisions, including Plutonium Materials and Technology (PMT), Theoretical (T), Materials Science and Technology (MST), and Chemistry (C).

In this issue of *Actinide Research Quarterly*, nine of our Seaborg postdocs write about their actinide science research.

Albert Migliori

Associate Director, Seaborg Institute

PING YANG

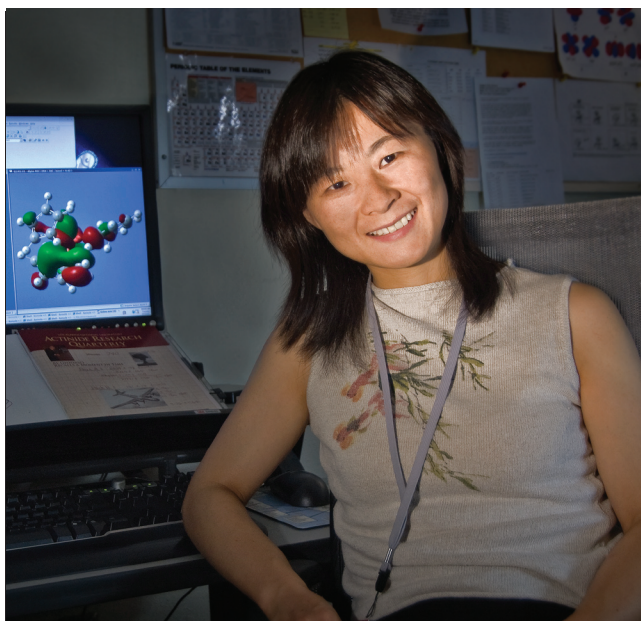
THEORETICAL STUDIES
OF BOND-ACTIVATION CHEMISTRY

The thorium(IV) and uranium(IV) alkyl complexes $(C_5Me_5)_2AnR_2$, where the actinide (An) is thorium (Th) or uranium (U) and the alkyl (R) is a methyl (CH_3), a benzyl (CH_2Ph), or a phenyl (Ph), have proven to be versatile starting materials for the synthesis of a diverse array of actinide organometallic systems containing actinide–nitrogen (An–N) bonds such as imido, hydrazonato, and ketimido complexes, which feature novel electronic properties.

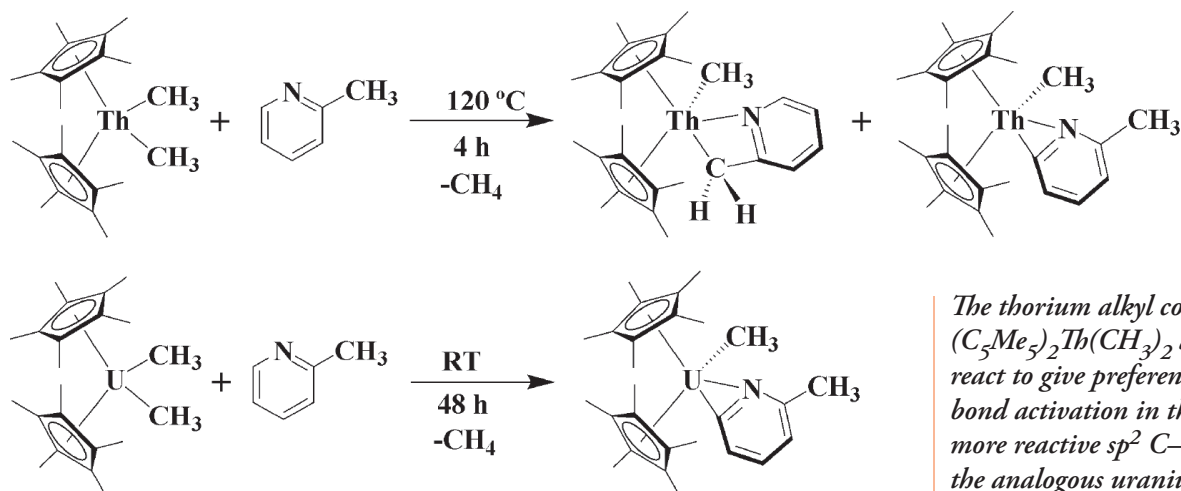
Recently, a group led by Jaqueline Kiplinger of Condensed Matter and Thermal Physics (MPA-10) reported that these actinide alkyl complexes undergo interesting carbon–hydrogen (C–H) and carbon–nitrogen (C–N) bond cleavage chemistry with N-heterocycles, such as 2-picoline (2-methylpyridine), which possesses both sp^2 and sp^3 hybridized C–H bonds. The sp^2 bond is hybridized from one s orbital and two p orbitals, resulting in a trigonal planar structure. The sp^3 bond is formed as a hybrid of one s and three p orbitals, resulting a tetrahedral shape.

The thorium alkyl complex $(C_5Me_5)_2Th(CH_3)_2$ activates both an sp^3 C–H bond on the 2-picoline methyl group and an *ortho* sp^2 C–H bond on the ring, producing the kinetic α -picolyl product, $(C_5Me_5)_2Th(CH_3)[\eta^2-(N,C)-2-CH_2-NC_5H_3]$, and the thermodynamic η^2 -pyridyl product, $(C_5Me_5)_2Th(CH_3)[\eta^2-(N,C)-6-CH_3-NC_5H_3]$, respectively. This is in marked contrast with the uranium system, which only reacts with an sp^2 C–H bond on the 2-picoline aromatic ring, producing the η^2 -pyridyl product $(C_5Me_5)_2U(CH_3)[\eta^2-(N,C)-6-CH_3-NC_5H_3]$. Deuterium-labeling studies demonstrated that the thorium and uranium

Ping Yang works in the Theoretical Division's Theoretical Chemistry and Molecular Physics Group (T-12). She received her doctorate in computational chemistry from Michigan Technological University in 2005. Yang began her postdoctoral appointment in January 2006. Her mentors are Richard Martin and P. Jeffrey Hay of T-12.



Larry Gibbons



The thorium alkyl complex $(C_5Me_5)_2Th(CH_3)_2$ and 2-picoline react to give preferential sp^3 C–H bond activation in the presence of a more reactive sp^2 C–H bond, while the analogous uranium complex, $(C_5Me_5)_2U(CH_3)_2$, reacts with only the ortho 2-picoline sp^2 C–H bond.

$(C_5Me_5)_2An(CH_3)_2$ complexes react with 2-picoline by different mechanistic reaction pathways.

Density functional theory methods have been employed to explore actinide–ligand interactions in a variety of complexes using the current generation of hybrid functionals. The structures, thermochemistry, and spectroscopic properties revealed through density functional theory provide information to compare with available structural and spectroscopic data from experiment. By comparison, relatively little information has been available on reaction mechanisms of f-element complexes, such as in the C–H activation processes.

Working with Los Alamos colleagues Richard L. Martin and P. Jeffrey Hay, and Ingolf Warnke of the University of Saarland, Germany, I performed a computational study of the competitive sp^2 versus sp^3 C–H activations within the same reactant molecule. Th(IV) complexes possess a closed shell electronic ground state ($5f^0$), while U(IV) systems represents a high-spin ($5f^2$) system with two unpaired electrons in f orbitals. The products and resulting thermochemistry in these reactions were compared and likely reaction precursors and transition states were also identified, as well the plausible reaction pathways.

The results of theoretical study are consistent with reported experimental results. Optimized geometries are in excellent agreement with X-ray crystal data. The calculated reaction energies prove that sp^2 C–H bond activation product is the most stable structure, i.e., thermodynamic product. Both theoretical and experimental observations point to the same conclusion: in the thorium system, the sp^3 product is kinetic and the sp^2 product is thermodynamic; while in the uranium system, the sp^2 product is both kinetic and thermodynamic.

In summary, the reaction initiates from formation of a weakly bound adduct, followed by the activation of adjacent C–H activation by an actinide center leading to an agostic transition state. My colleagues and I found that the actinide atom plays a fundamental role during the hydrogen migration process from

2-picoline to the methyl-leaving group. Agostic five-centered transition structures for the actinide C–H activation reaction pathways are reported to the best of our knowledge, for the first time. The origin of the regioselectivity of these reactions rests in these highly ordered configurations of transition states. Despite many common features found between thorium and uranium systems, including the similar geometries of the products, adducts, and the agostic transition states, the calculated activation energies between sp^2 and sp^3 activation differ slightly. For the thorium system, the sp^2 activation energy is higher than that for the corresponding sp^3 reaction. In contrast, for the uranium system, the sp^2 activation energy is lower than that for the corresponding sp^3 reaction.

On the basis of the combination of labeling, structural, and computational information, we proposed a general mechanism for the C–H activation of N-heterocycle by actinocene complexes. “Agostic migration” cyclometalation is indicated as an operative mechanism.

The calculated three-dimensional structures of the transition states involved in the sp^2 and sp^3 C–H bond activation of 2-picoline from the most stable thorium and uranium adducts.

	sp^2 activation	sp^3 activation
Complex		
Thorium		
Uranium		

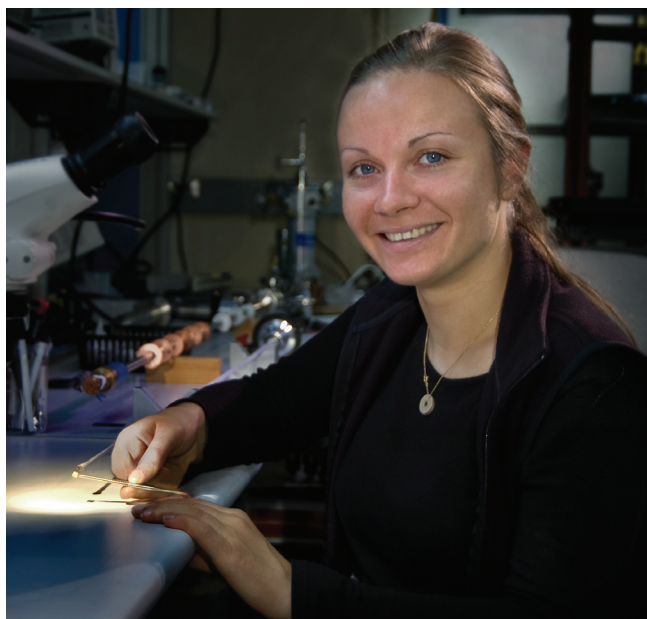
SONIA FRANCOUAL

THE EFFECTS OF RHENIUM DOPING ON THE TEMPERATURE-VERSUS-HIGH MAGNETIC FIELD PHASE DIAGRAM OF URU₂SI₂

Heavy fermions are actinide or rare-earth intermetallic alloys in which the hybridization between the localized f electrons and the conduction electrons yields strong correlations that cause important renormalization of the Fermi surface at low temperature. The primary electron–electron interactions at play are the local Kondo interaction associated with the screening of a virtual f-magnetic impurity by the conduction electrons and the indirect exchange long-range RKKY interaction between f magnetic moments. (RKKY stands for Ruderman-Kittel-Kasuya-Yosida and refers in a metal to the interaction of magnetic spins mediated by conduction electrons.)

These two interactions compete, yielding heavy fermion behavior and magnetic ordering, respectively. The fragile balance between the two interactions can be tuned by an external parameter such as pressure, magnetic field, or chemical doping, all of which may induce a quantum phase transition at absolute zero into a magnetically ordered state. On the way to and away from the transition, a variety of unusual electronic and magnetic behaviors is observed, from non-Fermi liquid behavior to unconventional superconductivity.

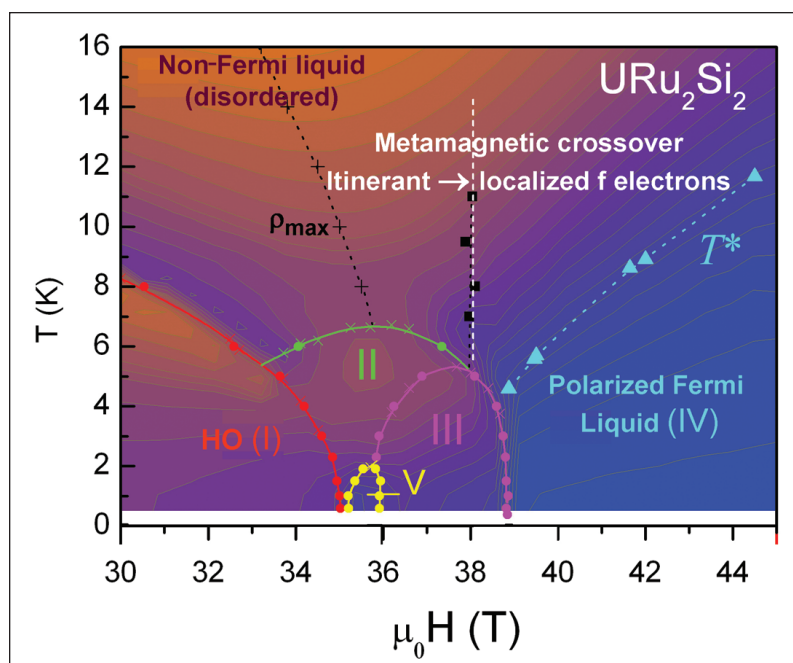
The uranium-ruthenium-silicon compound URu₂Si₂ is a moderately heavy electron compound crystallizing in the I4/mmm body-centered tetragonal structure of the thorium-chromium-silicon compound ThCr₂Si₂. At temperatures above the coherence temperature of 80 kelvin (K), the conduction



Larry Gibbons

Sonia Francoual works in the Materials Physics and Applications Division's National High Magnetic Field Laboratory (MPA-NHMFL). She received her doctorate from Joseph Fourier University, Grenoble, France, in April 2006. Her thesis was titled "Phonons and phasons in icosahedral quasicrystals and their 1/1 periodic approximants." Francoual began her postdoctoral appointment in June 2006. Her mentors are Neil Harrison and Alex Lacerda of MPA-NHMFL.

Sonia Francoual thanks Neil Harrison, Alex Lacerda, Marcelo Jaime, and Charles Mielke of the National High Magnetic Field Laboratory, Los Alamos; and Nicholas Butch and M. Brian Maple of the University of California, San Diego for their contributions to this article.



A temperature-versus-high magnetic field phase diagram of URu_2Si_2 obtained from resistivity versus H and T data (Kim, Harrison, Jaime, and others in *Physical Review Letters* 91, 2003). Solid-colored circles denote phase transitions with region I referring to the hidden-order phase and regions II, III, and V constituting new phases. “+” symbols signal a broad maximum observed at high temperature in the field dependence of the magnetoresistance. “■” symbols denote the metamagnetic transition field obtained from magnetization data (Harrison, Jaime, and Mydosh in *Physical Review Letters* 90, 2003).

surate spin excitations and of the absence of crystalline electric field excitations below 10 millielectronvolts (Wiebe, Janik, MacDougall, and others in *Nature Physics* 3, 2007) and the recent field- and temperature-dependent measurements of the Hall Effect (Oh, Kim, Sharma, and others in *Physical Review Letters* 98, 2007) unveil important changes of the Fermi surface topology at the transition pointing toward an itinerant density-wave type order parameter.

In heavy-electron systems, the application of a magnetic field leads to the progressive breaking of the hybridization between the f electrons and the conduction electrons upon the alignment along the magnetic field of the spin degrees of freedom of the f quasiparticles. Their complete polarization suggests recovering of the full moment μ_B per f atom and is accompanied by a dramatic increase of the magnetization. The phenomenon—called itinerant electron metamagnetism—has been observed in URu_2Si_2 as has the non-Fermi liquid behavior associated with the putative existence of a quantum critical point at absolute zero between the low-field paramagnetic hidden-order-phase and the high-field polarized Fermi liquid.

A remarkable situation in URu_2Si_2 is that the divergence of the fluctuations expected at the quantum critical point is avoided, and multiple-field-induced ordered phases form instead, as shown in the figure at left. The ordering at the quantum critical point has been “ascribed to reentrant phenomena arising from the interplay of itinerant electron metamagnetism and the hidden order parameter as the hidden-order phase is suppressed at 36 T [tesla],” (Harrison, Jaime, and Mydosh in *Physical Review Letters* 90, 2003). An extensive body of research in strong magnetic fields has been carried out in URu_2Si_2 over the past five years

electrons are scattered by isolated spins. At temperatures below 80 K, the Kondo lattice regime in which the resistivity becomes Fermi-liquid-like prevails and the mass enhancement due to electron correlations is approximately $25 m_e$ (m_e being the mass of the free electron). At lower temperatures, URu_2Si_2 orders with a transition at 17.5 K into a hidden-order (HO) phase presenting a small antiferromagnetic moment of $0.03 \mu_B$ (μ_B stands for Bohr magneton, the unit used to express the electron magnetic dipole moment) and finally a transition at 1.2 K into a superconductive phase.

The transition at 17.5 K is abrupt and is observed in several measurable physical quantities such as resistivity, magnetic susceptibility, specific heat, thermal expansion, thermoelectric power, and thermal conductivity. However, the order parameter in the hidden-order phase remains unidentified. The recent neutron scattering observations of the gapping of itinerant-like incommen-

to determine on one hand the properties of the Fermi liquid upon which the ordering manifests and on the other hand the nature of the ordering at high field in relation to the hidden order at low field.

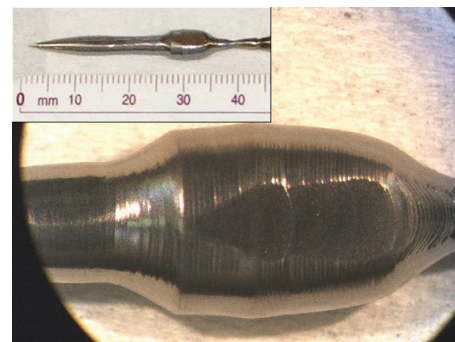
A 5-percent-or-less transition-metal substitution of ruthenium atoms in URu_2Si_2 suppresses the hidden order at 17.5 K, while the overall heavy-electron behavior is preserved. Studies of the combined effects of rhodium doping and applied magnetic field reveal that the ordering in URu_2Si_2 at high field is significantly modified with the development of a single-field-induced robust phase (namely phase II in the figure on the previous page) around the putative quantum critical point located at approximately 34 T in $\text{URu}_{1.92}\text{Rh}_{0.08}\text{Si}_2$.

At low field, a heavy Fermi liquid appears where the hidden order is suppressed. Those properties follow the addition and the removal of conduction electrons associated with the transition-metal substitution and the modifications of the degree of hybridization between the f electrons and the conduction electrons of the ligand transition-metal atoms.

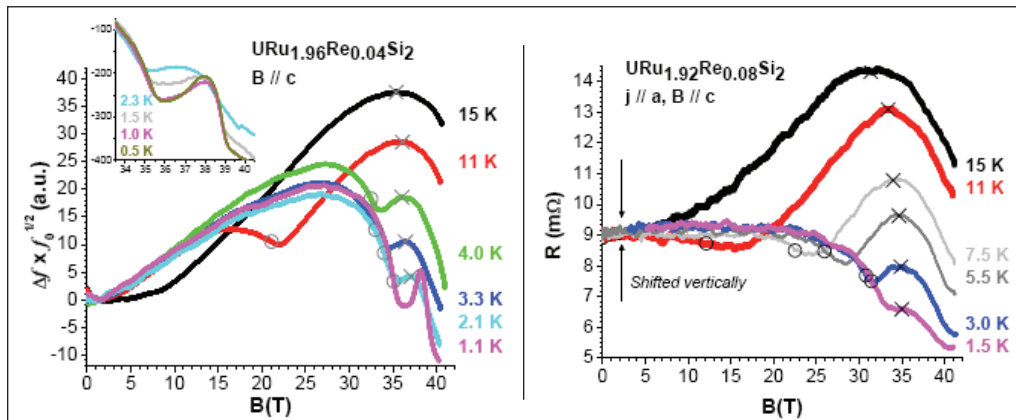
More-substantial transition-metal substitutions yield a complex magnetism that can be either antiferromagnetic ordering (rhodium, palladium, iridium, and platinum) or itinerant ferromagnetism (rhenium, technetium, and manganese), depending on the nature of the transition-metal element. Of particular recent interest is the doping of URu_2Si_2 with rhenium as ferromagnetic order develops for substitutions above 15 percent at which order coexists with non-Fermi liquid behavior at temperatures below 14 K.

In this research project, the high magnetic field phase diagram of $\text{URu}_{2-x}\text{Re}_x\text{Si}_2$ single crystals is mapped by magnetoresistance and magnetization measurements at low temperature in pulsed magnetic fields at the National High Magnetic Field Laboratory in Los Alamos. An accurate determination of the position in field and temperature of the phase transitions as a function of the rhenium doping was made on each sample through resistivity and magnetization measurements. Brian Maple and his group at the University of California, San Diego grew the samples. Maple's group combined high-purity uranium, ruthenium, rhenium, and silicon via arc melting in an argon atmosphere to grow polycrystals from which single crystals were produced using the Czochralski method in a tri-arc furnace under flowing argon. The crystal quality and lattice parameters were confirmed by X-ray powder diffraction.

The crystals have a plane-parallel shape of approximately 0.7 x 1.7 millimeters (mm), the longer edge being along the easy axis of magnetization c. The thickness is limited to 0.2 mm to avoid magnetocaloric effects and Joule heating of the sample during the pulse. Because the measured zero-field resistance of some of the samples is on the order of 5 milliohms ($\text{m}\Omega$) or less at 4 K, the standard method of four-wire resistivity measurement in pulsed field becomes challenging. The alternative contactless tunnel diode oscillator technique consists of measuring the change in frequency and amplitude of the circuit oscillations of a self-resonant radio-frequency tank circuit composed of a coil (inductor) in the center of which the sample is placed.



A single crystal of the heavy fermion superconductor URu_2Si_2 lightly doped with rhenium. The cylindrical sample was grown at the University of California, San Diego in Brian Maple's laboratory by Nick Butch and Ben Yukich using the Czochralski method in a tri-arc furnace under argon. The closeup shows a macroscopic flat face parallel to the tetragonal basal plane.



Magnetoresistance curves measured at several different temperatures in $URu_{1.96}Re_{0.04}Si_2$ using the tunnel diode oscillator (TDO) technique in the 50-tesla (T) mid-pulse magnet at the Los Alamos National High Magnetic Field Laboratory are shown in the figure above left. The sample is oriented with the c axis aligned with the magnetic field B . “ \times ” and “ \circ ” symbols mark the field position of the resistivity maximum and the exit from the hidden-order phase, respectively. TDO magnetoresistance curves at low temperatures shown in the 33–41 T narrow magnetic field range are shown above left. Magnetoresistance curves measured at several different temperatures in $URu_{1.92}Re_{0.08}Si_2$ using the four-wire standard technique in the 50-T mid-pulse magnet are shown in the figure above right. The sample is oriented such as the c axis is aligned with the magnetic field B and the current j is along the a axis. Curves have been shifted vertically in the aim of visual comparison with the TDO magnetoresistance curves in the figure above left.

proportional to the sample conductivity.

The tunnel diode oscillator experiments were carried out in a capacitor-driven 15-mm-bore 50-T nondestructive mid-pulse magnet. In this magnet, the 10-turns 1.9 mm-diameter compensated copper coil sits orthogonal to the magnetic field at the center of the field on the bottom part of a 1.5-m stick probe inserted in a helium-3 refrigerator. The tunnel diode, which is built into the probe, lies approximately 50 centimeters (cm) above the field center; the rest of the radio-frequency tank circuit sits outside of the helium-3, helium-4, and magnet spaces at a distance of approximately 1 meter (m).

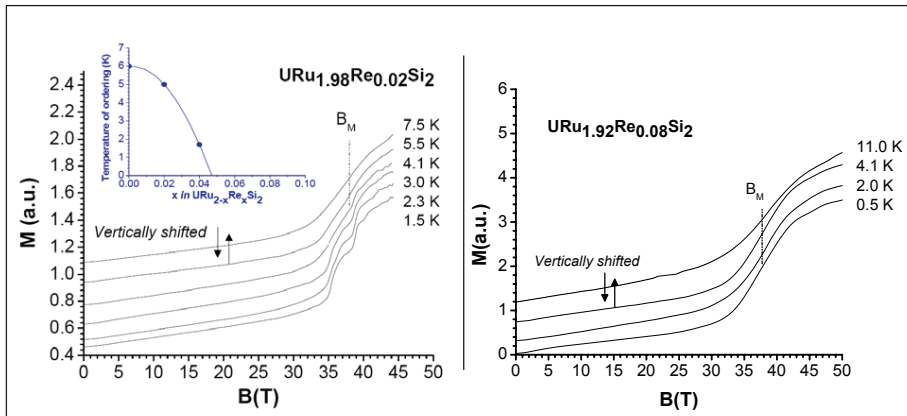
The radio-frequency circuit, set at an initial frequency of 200 kilohertz (kHz), allows absolute value frequency variations up to 200 kHz. The 2.5-megahertz upper digitizing frequency of the computer-controlled data acquisition card samples the time-dependent oscillatory behavior of the output signal.

The figures above the magnetoresistance curves measured on the falling field of the pulse at several different temperatures in $URu_{1.96}Re_{0.04}Si_2$ using the tunnel diode oscillator technique and in $URu_{1.92}Re_{0.08}Si_2$ using the four-wire technique. (In the latter case, the sample has a bar-like shape elongated along the a tetragonal axis and a 10-m Ω resistance at 5.5 K).

The magnetization measurements were carried out using a wire-wound sample-extraction magnetometer. Two measurements were performed consecutively, one with the sample inserted in (coupled to) the detection coil and a second with the sample removed from the coil, enabling a fully compensated signal. The magnetization curves measured on the falling field in $URu_{1.98}Re_{0.02}Si_2$ and $URu_{1.92}Re_{0.08}Si_2$ are displayed in the figures on the next page. For all measurements, the sample was mounted and oriented so that the c axis was aligned with the field and the sample lay at the center of the field. The temperature was reduced to 0.5 K by pumping on the helium-3 and -4 baths and heated to 20 K by a heater placed close to the sample.

Quantum criticality is evidenced by the presence of a broad maximum in the field dependence of the magnetoresistance, the position of which (when followed in temperature) enables one to extrapolate the position of the quantum

Whereas the four-wire method gives direct access to the resistance through an AC excitation current being passed through the sample and an AC potential difference measured across the sample, changes in the tunnel diode oscillator resonant frequency measure changes in the depth of the radio-frequency field penetrating the sample, which is inversely



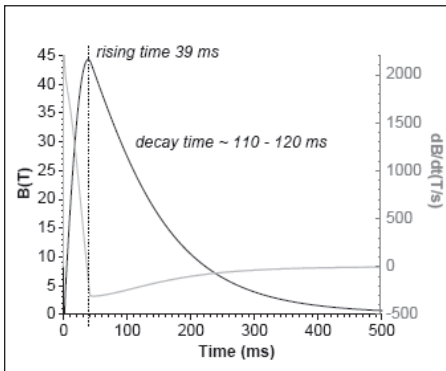
critical point at zero temperature. In the $\text{URu}_{2-x}\text{Re}_x\text{Si}_2$ samples studied ($x < 10\%$), this quantum critical (disordered) region is clearly identified in the magnetoresistance curves, a broad maximum emerging at fields around 34 T at 15 K, the width of which narrows and the position of which slightly shifts as the temperature is decreased.

This maximum can be followed down to 2.1 K in $\text{URu}_{1.96}\text{Re}_{0.04}\text{Si}_2$ and down to 0.5 K in $\text{URu}_{1.92}\text{Re}_{0.08}\text{Si}_2$. In $\text{URu}_{1.96}\text{Re}_{0.04}\text{Si}_2$, the sharpening and discontinuous shift and increase in magnitude of this maximum signal the entrance into an ordered phase at 1.7 K. The hidden-order phase associated at zero field with an enhancement of the resistivity below 15 K and 12 K for $x = 0.04$ and 0.08 in $\text{URu}_{2-x}\text{Re}_x\text{Si}_2$, respectively, clearly appears in the magnetoresistance curve at fields up to approximately 35 T and approximately 31 T as shown in the figures on the previous page.

Although the increase in resistivity in the hidden order relative to the increase in the quantum critical region is considerably reduced from 0.04 to 0.08, the field required to suppress the hidden order, although reduced, remains high. Itinerant electron metamagnetism manifests in URu_2Si_2 as a large increase in the magnetization at a field B_m of 38 T above a cut-off critical temperature (T_c) of 6 K. At lower temperatures, successive magnetization plateaus (spin-flip-like features) appear inside the metamagnetic crossover region as the consequence of successive phase transitions between different ordered phases (II, III, IV, V in the figure on page 6).

The metamagnetic transition is shown to survive for substitutions of the ruthenium atoms by rhenium up to 4% ($x = 0.08$). However, the magnetization plateaus observed at $x = 0.02$ below 5.0 K and at $x = 0.04$ below 2.0 K are not observed at $x = 0.08$ down to 0.5 K in agreement with the magnetoresistance measurements. B_m as obtained from a fit of the centered position of a single broad maximum in the differential susceptibility, moves to higher fields as the rhenium content increases, with B_m at 7.5 K approximately 37.3 (0.5) T at $x = 0.02$ and approximately 38.5 (0.5) T at $x = 0.08$. This rise is consistent with a proposed qualitative picture in which the low rhenium doping contributes

Field dependence of the magnetization in $\text{URu}_{1.98}\text{Re}_{0.02}\text{Si}_2$ measured at several different temperatures in the 50-tesla (T) mid-pulse magnet is shown in the figure at far left. The sample is oriented such that the c axis is aligned with the magnetic field B . Curves have been shifted vertically for clarity. The metamagnetic transition shows up at high temperatures as a broad magnetization increase for fields above 34 T. Below 4.0 kelvin (K), step-like features associated with phase transitions can be seen. Higher temperatures at which phase transitions are observed in the metamagnetic crossover region in the magnetization curves as a function of the rhenium doping in $\text{URu}_{2-x}\text{Re}_x\text{Si}_2$ are shown in the far left insert. Field dependence of the magnetization in $\text{URu}_{1.92}\text{Re}_{0.08}\text{Si}_2$ measured at several different temperatures in the 65-T short-pulse magnet is shown in the figure at near left. The sample is oriented such that the c axis is aligned with the magnetic field B . Curves have been shifted vertically for clarity. The metamagnetic field B_m at 7.5 K is centered at 38.50 (0.5) T in $\text{URu}_{1.92}\text{Re}_{0.08}\text{Si}_2$, whereas in the figure at far left it is centered at 37.3 (0.5) T in $\text{URu}_{1.98}\text{Re}_{0.02}\text{Si}_2$. Step-like features in the magnetization curves down to 0.5 K are not observed for this composition.



The time dependence of the magnetic field for a 45-tesla (T) shot fired in the 50-T mid-pulse magnet at the Los Alamos National High Magnetic Field Laboratory.

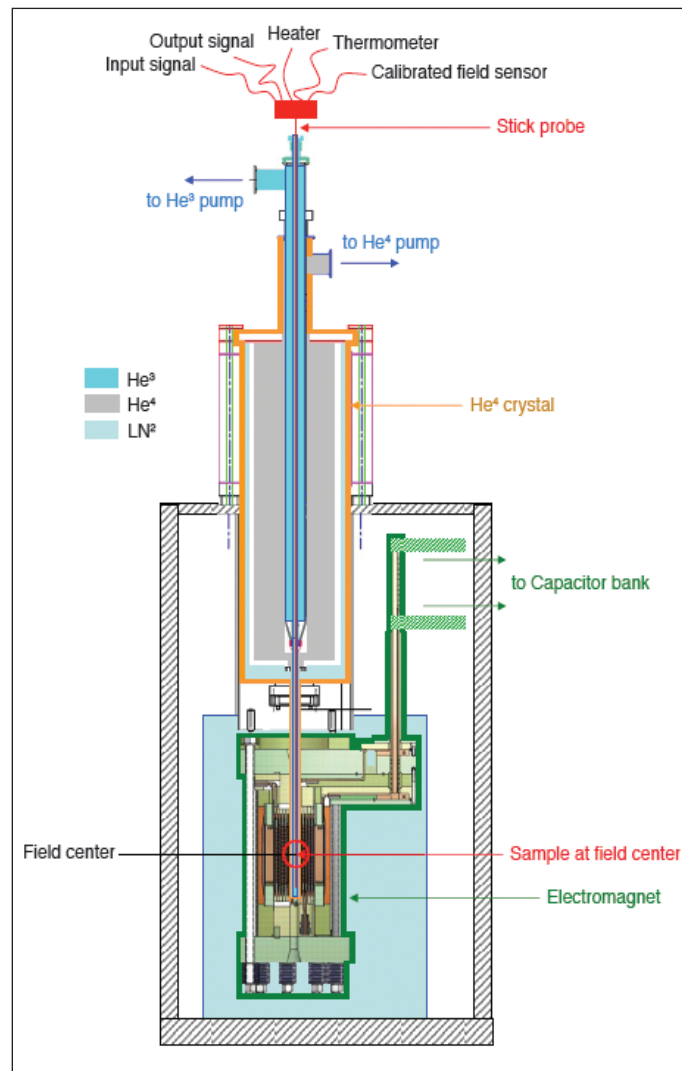
The experimental setup for the pulse-field measurements. (Schematic adapted from drawings by Ruminer and Swenson of the Los Alamos National High Magnetic Field Laboratory.) The oriented sample sits on the bottom of a 1.5-meter-long stick probe that is loaded into a helium-3 refrigerator and then inserted into a helium-4 cryostat. The temperature is tuned down to 0.5 kelvin (K) pumping on the helium-3 and -4 baths and heated to 20 K by applying a small amount of power on a heater situated close to the sample. A calibrated thermometer placed close to the sample measures the temperature before the pulse. The sample is placed at the center of the magnetic field at the beginning of the experiment. The magnetic field is measured during the pulse by means of a calibrated sensor coil placed close to the sample.

additional electrons to the system, making it more itinerant, and higher fields are required to break a strengthened hybridization between the f quasiparticles and the conduction band.

Marked differences are observed in the high-field phase diagram of URu_2Si_2 under rhenium doping as compared with the reported rhodium case. A progressive reduction in the ordering regions around the quantum critical point occurs as the rhenium content is increased, implying a complete suppression of the ordering at a rhenium doping of $x \sim 0.05$, suppression that becomes complete at $x = 0.08$. The underlying heavy Fermi liquid is one in which for $x < 0.10$ the f electrons gain in itinerancy, the opposite trend being observed in the rhodium case.

The present study sheds light on the effect of low transition-metal substitutions (rhenium doping versus rhodium doping on the ruthenium sites,

$x < 0.10$) on the formation of novel-ordered phases near the quantum critical point in the heavy-fermion compound URu_2Si_2 . We are now investigating how higher rhenium substitutions (between $x = 0.10$ and $x = 0.30$) that lead to the unusual coexistence of non-Fermi liquid behavior and emerging ferromagnetic order at zero field modify the itinerant electron metamagnetism properties and the spectrum of the quantum critical fluctuations at high magnetic field.



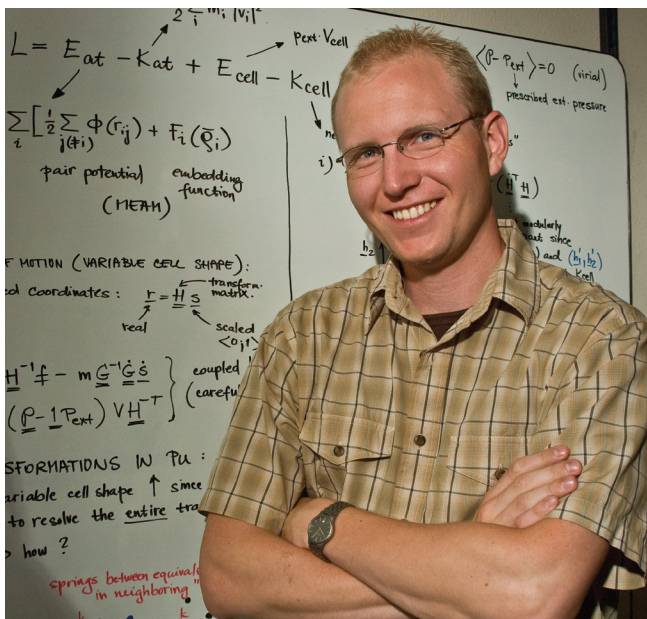
ROMAN GRÖGER

CHAIN-OF-STATES ATOMISTIC CALCULATIONS OF THE PATHWAYS AND ENERGETICS OF STRUCTURAL PHASE TRANSFORMATIONS IN PLUTONIUM

Understanding structural phase transformations in plutonium is an important step toward obtaining thermodynamic and kinetic descriptions of this material. At ambient pressures, plutonium exists in six crystal structures that range from the highly symmetric face-centered cubic δ phase with four atoms per unit cell to one of the least symmetric structures: the monoclinic low-temperature α phase with 16 atoms per unit cell. Just above room temperature, plutonium transforms to its body-centered monoclinic β phase whose unit cell is experimentally predicted to consist of 34 atoms, an unusual number.

Some insight into the nature of the phase transformations between various allotropes of plutonium has been gained recently using the Modified Embedded Atom Method (MEAM). These calculations not only correctly predict the order of the crystal structures and their stabilities but also reproduce the large 25% volume difference between the α and δ phases. However, the time scale required for observing a phase transformation between two phases is typically beyond the reach of conventional molecular dynamics simulations.

To probe the structural phase transformations in plutonium, we use a chain-of-states calculation implemented within the so-called nudged elastic band (NEB) method. We consider a chain of states $\{0, 1, 2, \dots, M+1\}$ of $M+2$ replicas (images) of the system, that is a discrete representation of the transformation



Roman Gröger works in the Theoretical Division's Statistical Physics and Condensed Matter Group (T-11) and the Center for Nonlinear Studies (CNLS). He received his doctorate in engineering mechanics from Brno University of Technology and Academy of Sciences of the Czech Republic in 2003 and his doctorate in materials science from the University of Pennsylvania in 2007. Gröger began his postdoctoral appointment in February 2007. His mentor is Avadh Saxena of T-11.

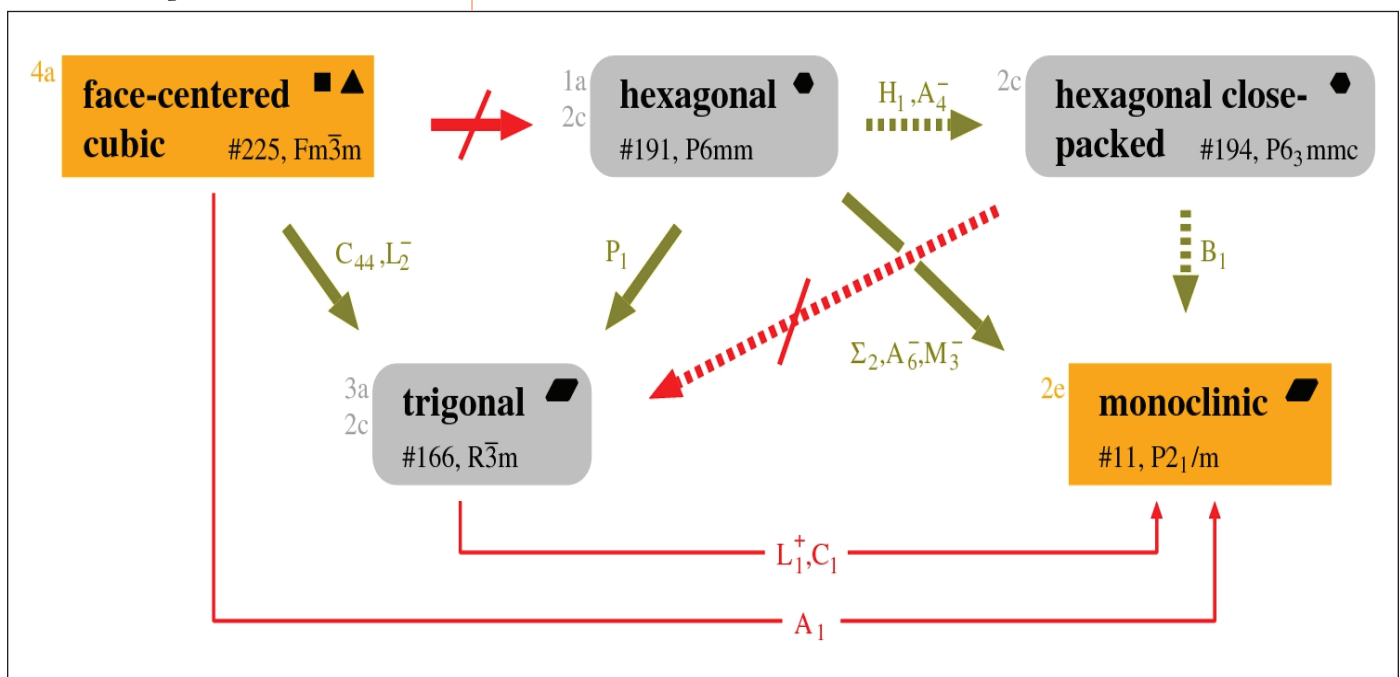
Larry Gibbons

The phonon mechanism for $\delta \leftrightarrow (\alpha)$ α' phase transformation proposed by Turab Lookman, Avadh Saxena, and Robert Albers is shown below. The green arrows indicate displacive (martensitic) transformations between structures that are group-subgroup related. The crossed red arrows show reconstructive transformations between structures without any group-subgroup relation. An exhaustive search reveals that the displacive transformation between the face-centered cubic and monoclinic phases proceeds via intermediate trigonal and hexagonal structures. The labels attached to individual arrows indicate specific phonons that drive the corresponding transformation; the Wyckoff symbols of each structure are attached to the left of each box. (A Wyckoff symbol determines positions and multiplicity of atoms in the unit cell, e.g., "2c" means two atoms in the c positions.)

pathway. The atoms in the images 0 and $M+1$ are fixed and correspond to the initial and the target states of the system, while the remaining M movable images form the so-called elastic band. The atomic structure of each image is determined by the $3N$ positions of atoms, each of which is connected to its counterpart in the neighboring image by a linear spring to obtain a discrete representation of the transformation pathway. The coordinates of atoms in the M intermediate images are then determined by minimizing the total potential energy, represented by the objective function

$$\mathcal{S}(\{\mathbf{r}_{j=1,\dots,N}^{(i=0,\dots,M+1)}\}) = \sum_{i=1}^M E(\{\mathbf{r}_1^{(i)}, \dots, \mathbf{r}_N^{(i)}\}) + \sum_{i=1}^{M+1} \sum_{j=1}^N \frac{1}{2} k [\mathbf{r}_j^{(i)} - \mathbf{r}_j^{(i-1)}]^2$$

with respect to the positions of atoms in images. The potential energy E of every image i can be calculated readily by using empirical or semi-empirical potentials, in our case the MEAM potential for plutonium. The relaxed configuration corresponds to zero forces on all atoms due to the interatomic potential and is largely independent of the choice of the spring constant k . The obtained coordinates of atoms in images 1 to M can be used to search systematically for the symmetry, space group, and Wyckoff positions by using the Rietveld refinement. Importantly, the variation of the potential energy E along the elastic band provides a direct measure of the energy barrier that has to be surmounted to transform between the given crystal structures.



Plutonium crystal structure

These are the six ambient-temperature phases of plutonium and their crystal lattice structures:

α	alpha	simple monoclinic
β	beta	body-centered monoclinic
γ	gamma	face-centered orthorhombic
δ	delta	face-centered cubic
δ'	delta prime	body-centered tetragonal
ϵ	epsilon	body-centered cubic

The main goal of this project is to couple the NEB method with the semi-empirical MEAM potential for plutonium to elucidate the mechanism of structural phase transformations in elemental plutonium and its dilute alloys. The current calculations aim to determine the energy barriers for $\alpha \leftrightarrow \beta$, $\beta \leftrightarrow \gamma$, $\gamma \leftrightarrow \delta$, and $\delta \leftrightarrow \epsilon$ phase transformations that are required for reliable formulation of the activation enthalpies and the free-energy functional of plutonium. The calculations of the energy barriers for $\alpha \leftrightarrow \beta$ with the β structure containing both 32 and 34 atoms and the subsequent comparison of the calculated photoemission spectra with experimental measurements will shed new light on the still controversial structure of the β phase.

Moreover, Los Alamos researchers Turab Lookman, Avadh Saxena, and Robert Albers of the Statistical Physics and Condensed Matter Group have recently proposed a phonon mechanism for the $\alpha(\alpha') \leftrightarrow \delta$ phase transformation in plutonium that is based purely on symmetry relations (group–subgroup) and which predicts an existence of intermediate trigonal and simple hexagonal phases. The existence of these intermediate structures, and thus the validity of this model, can be checked by examining the calculated transformation pathway between the α and δ phases. The same method will be used to investigate the influence of alloying on the transformation pathway and shape of the energy barrier between the α' and δ phases.

LINDSAY ROY

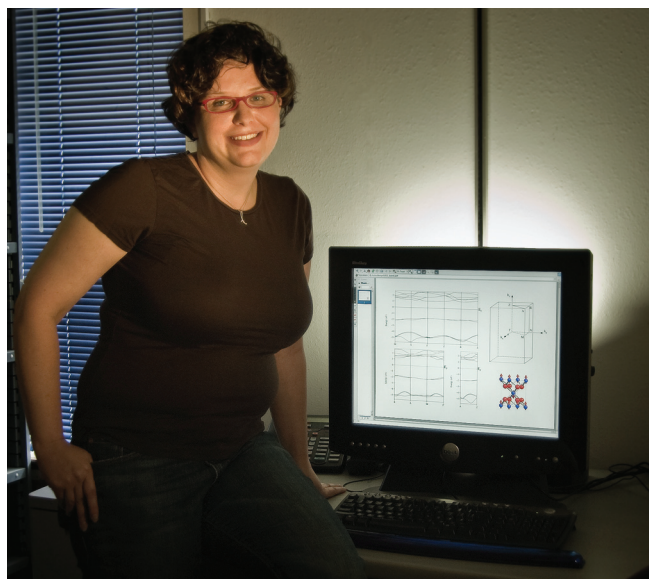
QUANTUM CHEMISTRY APPROACHES
TO ACTINIDE ELECTRONIC STRUCTURE

The corrosion reactions of uranium and transuranic metals represent a challenge for both experimentalists and theorists because of their chemical complexity, while presenting a serious concern for environmental preservation. The long-term storage of radioactive waste (containing mainly uranium and plutonium compounds) requires a comprehensive knowledge of the possible oxidation reactions that could occur. For example, plutonium crystallizes in seven distinct phases, is highly reactive, and can have five different oxidation states when forming compounds. The surface of metallic plutonium easily oxidizes to PuO_2 when exposed to air and moisture, while Pu_2O_3 plays an important role in oxidation kinetics.

Given the incomplete understanding of the plutonium-oxidation chemistry and the myriad problems associated with experimental studies on plutonium oxides, theory can provide fundamental insight into the electronic structure and properties of these systems.

Unfortunately, theoretical studies on these materials are quite difficult. The 5f electrons can either be localized or contribute to bonding, and their relativistic effects and electron–electron correlations are very important factors in deciding the degree of localization. In particular, actinide oxides (AnO_2) exhibit amazingly complex behavior despite having a simple binary formula because they straddle the metallic, ionic, and covalent bonding descriptions used by chemists and physicists. Because of this, previous theoretical studies on these materials using local spin-density approximation (LSDA) and generalized

Lindsay Roy works in the Theoretical Division's Theoretical Chemistry and Molecular Physics Group (T-12). She received her doctorate from Texas A&M University under the direction of Timothy Hughbanks, where her research focused on developing theoretical models for understanding the magnetic interactions in lanthanide-based molecules, clusters, and solids. She began her postdoctoral appointment in November 2006. Her mentor is Richard Martin of T-12.



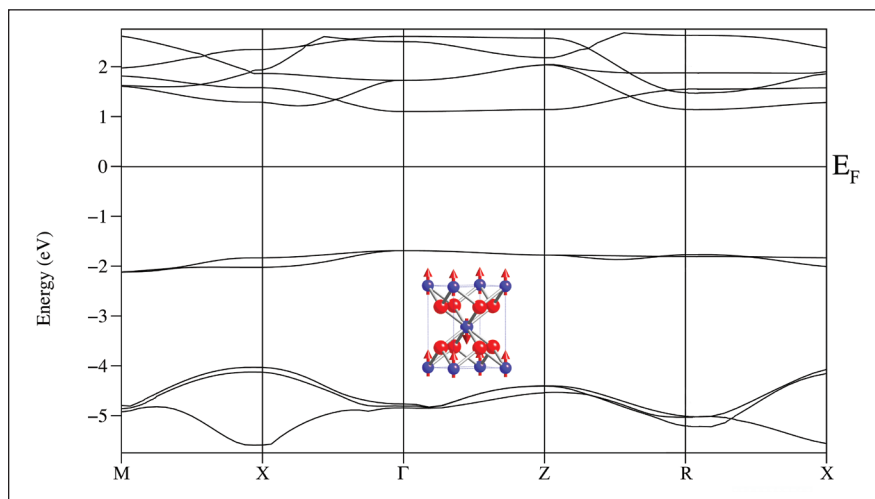
Larry Gibbons

gradient approximations (GGAs) of density functional theory fail to accurately describe the bonding and electronic structure of these compounds.

Recently, Richard Martin of Los Alamos' Theoretical Chemistry and Molecular Physics Group, Gustavo Scuseria of Rice University, and their coworkers have shown that a third generation of functionals, the hybrid density functional theory approximation that combines the exact, non-local, Hartree-Fock exchange interaction with the traditional local (LDA) or semi-local (GGA) exchange and correlation interactions, has been able to correctly predict a magnetic ground state, an insulating gap, and the lattice constants for the uranium oxide (UO_2) series.

Continuing the research, we have shown that the 5f orbitals are localized in the band structure of UO_2 but that there is small dispersion of approximately 300 millielectronvolts (meV). One might expect later members of the series to show even more localized character because the f-orbital radial extent decreases moving across the row. Interestingly, a 5f– O_2p orbital energy degeneracy occurs, which leads to significant orbital mixing and covalency in the intermediate region (PuO_2 – CmO_2), and ground state in curium oxide (CmO_2) prefers a half-filled f^7 subshell (Cm^{3+}) instead of the expected f^6 configuration (Cm^{4+}). Preliminary results of the band structure of PuO_2 reveal that there is some amount of mixing between the 5f and 2p bands. It will be interesting to see how the f–p mixing changes in CmO_2 , where the oxygen 2p atoms are donating spin density to the 5f to stabilize a half-filled subshell.

One caveat to previous calculations is the omission of spin-orbit coupling, or the interaction of the electron spin magnetic moment with the magnetic moment due to the orbital motion of the electron, which is significant for heavy atoms. Calculations of UO_2 with spin-orbit coupling show that the band gap decreases by 0.06 eV, but that spin-orbit coupling is a minor perturbation to the calculations. We are currently working on including spin-orbit coupling effects to the AnO_2 series.



Calculations of the uranium oxide (UO_2) band structure (large image) were performed on an antiferromagnetic tetragonal cell (inset). The red arrows in the inset represent the direction of the $5f^2$ electrons on each uranium atom. The oxygen p bands are well separated from the uranium f bands, and the occupied 5f bands show some dispersion and have a bandwidth of approximately 300 millielectronvolts.

MING TANG

RADIATION DAMAGE EFFECTS
IN URANIUM-BEARING DELTA-PHASE OXIDES

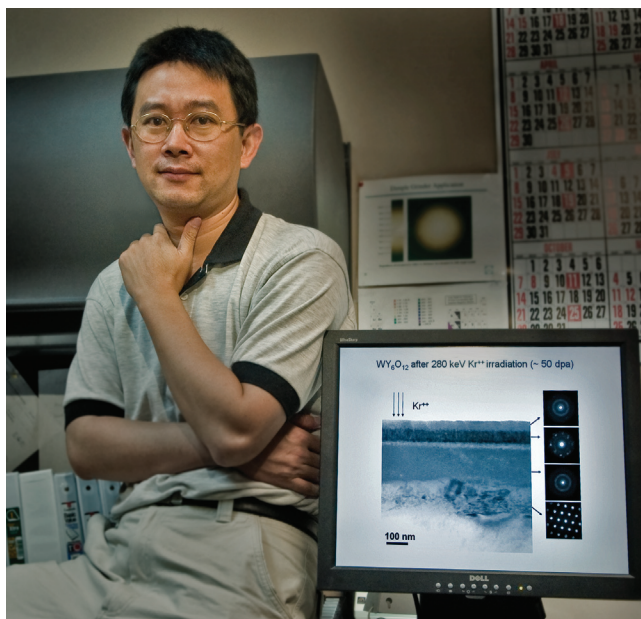
Actinide oxides have been used as nuclear fuel since the first controlled chain reaction in 1942. Today, the DOE is facing the disposal of vast quantities of spent uranium-oxide (UO_2) fuel that have accumulated over fifty years or more. Simultaneously, the DOE is positioning itself to coordinate the development of advanced nuclear fuels that may help to mitigate both nuclear materials disposal and proliferation problems.

More recently, the DOE has expressed an interest in the performance of non-metallic materials in hostile environments, especially the behavior of advanced ceramic nuclear fuel forms. UO_2 and mixed oxide (MOX) fuels, which crystallize in the fluorite structure, exhibit exceptional resistance to irradiation damage and are therefore the predominant fuel for thermal power reactors.

My research involves the synthesis and fabrication of complex ceramic oxide samples, which are fluorite structural derivatives of compounds with stoichiometries near to M_7O_{12} , namely, the so-called delta (δ) phase, made from mixtures of uranium oxide (both UO_2 and UO_3) and sesquioxide compounds such as Y_2O_3 . In addition, I am investigating the radiation damage behavior of these MOX fuels to determine the viability of these compounds for application as actinide-host nuclear fuel and waste forms.

My colleagues and I have recently shown that certain δ -phase oxides are extraordinarily radiation tolerant; in particular, they are especially resistant to amorphization transformations. Delta-phase compounds are also spacious

Ming Tang works in the Materials Science and Technology Division's Structure/Property Relations Group (MST-8). He received his doctorate in materials engineering in 2006 from the New Mexico Institute of Mining and Technology. Tang began his postdoctoral appointment in September 2006. His mentor is Kurt Sickafus of MST-8.

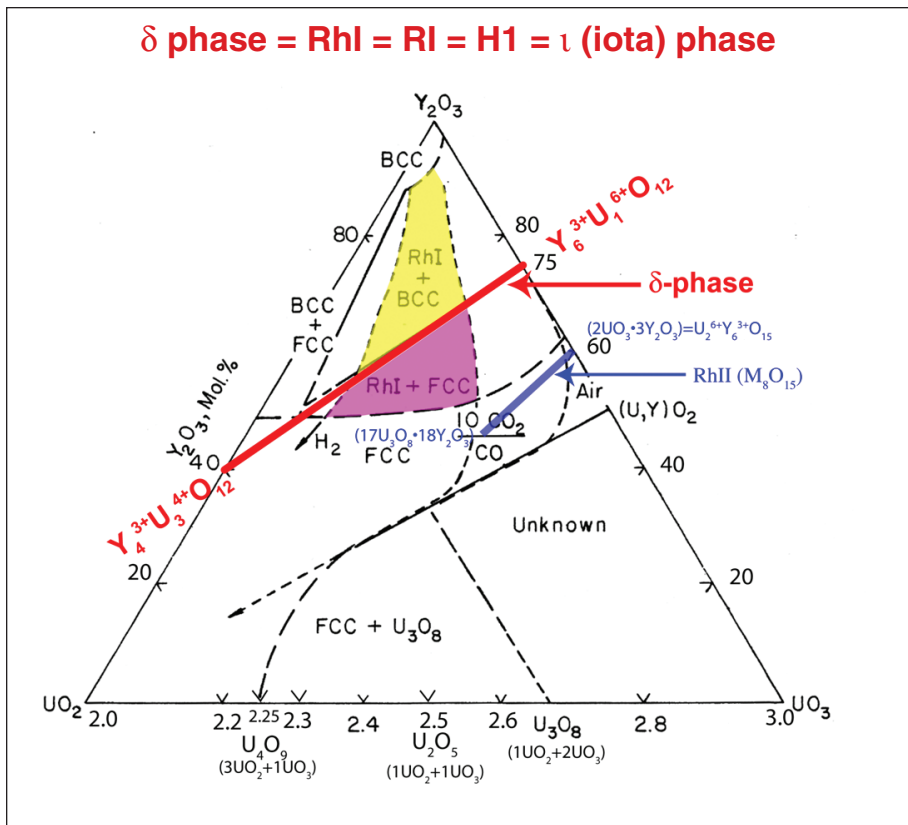


Larry Gibbons

(fluorite-derivative-structured) compounds that can readily accommodate actinides in their crystal lattices. The ability of the δ phase to accommodate actinides is illustrated in the $\text{UO}_2\text{-UO}_3\text{-Y}_2\text{O}_3$ phase diagram. In that system, the δ phase exists from a fully oxidized stoichiometry of $\text{Y}_6^{3+}\text{U}_1^{6+}\text{O}_{12}^{2-}$ to a fully reduced stoichiometry of $\text{Y}_4^{3+}\text{U}_3^{4+}\text{O}_{12}^{2-}$ (the red line in the phase diagram below).

The importance of compounds containing a mixture of U^{6+} and U^{4+} species is that such compounds are surrogates for waste forms or fuel forms that may contain a mixture of uranium and higher actinides. We envision that the δ phase may be used to incorporate a variety of actinides to produce compounds such as $\text{Y}_6^{3+}(\text{U}_x^{6+}\text{Pu}_y^{4+}\text{Am}_z^{4+})\text{O}_{12}^{2-}$.

One goal of this research is to understand trends in radiation damage behavior as one progresses from the fully oxidized δ -phase composition, $\text{Y}_6^{3+}\text{U}_1^{6+}\text{O}_{12}^{2-}$, to the fully reduced composition, $\text{Y}_4^{3+}\text{U}_3^{4+}\text{O}_{12}^{2-}$, to explain the paradoxical distinction between the radiation damage responses of seemingly similar materials. Another goal is to establish criteria that will enable scientists to predict the radiation-damage tolerance (or damage sensitivity) of specific ceramic compounds. Ultimately, my colleagues and I hope to discover new radiation-tolerant ceramics and develop these materials for application in hostile radiation environments, especially as actinide hosts for advanced nuclear fuels or wastes.



This three-component phase diagram shows the phase stability regions for mixtures of $\text{UO}_2\text{-UO}_3\text{-Y}_2\text{O}_3$. The red line indicates the compositional range for the M_7O_{12} delta (δ)-phase structure. The label in red above the diagram indicates the many names that have been ascribed to the δ phase in the literature over the years.

ROBYN GDULA

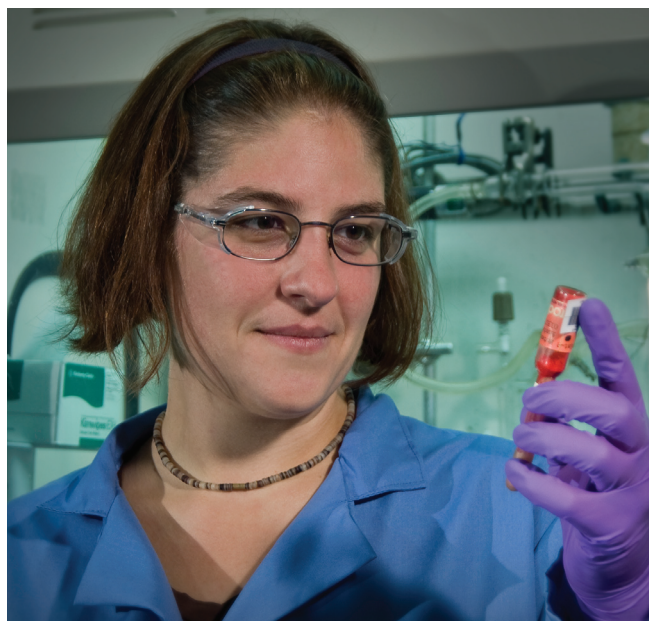
PROBING THE NATURE
OF URANIUM-LIGAND MULTIPLE BONDS

In 2005, Los Alamos researchers Trevor Hayton, James Boncella, Brian Scott, Phillip Palmer, Enrique Batista, and P. Jeffrey Hay reported the synthesis and characterization of two different uranium(VI) bis-imido species, $U(N^tBu)_2I_2(thf)_2$ and $U(NPh)_2I_2(thf)_3$, (**1**) and (**2**), respectively, in the illustration on the next page. Density functional theory calculations performed on these early structures displayed striking similarities to the uranyl species, $trans-UO_2X_4$, including the presence of a triple bond between the uranium (U) and nitrogen (N) atoms, similar to that between the uranium and oxygen atoms of uranyl.

However, the ordering of the energies for these two sigma (σ) and four pi (π) bonds is altered in the imido species, compared to those of the oxo species. Furthermore, the imido species are predicted to display more covalency in the U–N multiple bond than the analogous uranyl complexes because of the difference in electronegativity values between nitrogen and oxygen. I am exploring the novel reactivity observed with various bis-imido species due to these two factors.

Initially the synthetic route to **1** was explored, as it had only proven to work in this specific case. To test whether this was specific to the starting material, I substituted methylamine in place of *tert*-butylamine. Instead of yielding the expected bis-methylimido species, a uranium(VI)bis-imido cation (**3**) was isolated with a tri-iodide counterion, the first positively charged version of this species to be characterized. It was discovered that the *tert*-butyl version of the

Robyn Gdula works in the Materials Physics and Applications Division's Materials Chemistry Group (MPA-MC). She received her doctorate from the University of Michigan in 2006 under the direction of Marc J. A. Johnson. Her thesis project was the study of organometallic catalysis. Gdula began her postdoctoral appointment in July 2006. Her mentor is James Boncella of MPA-MC.



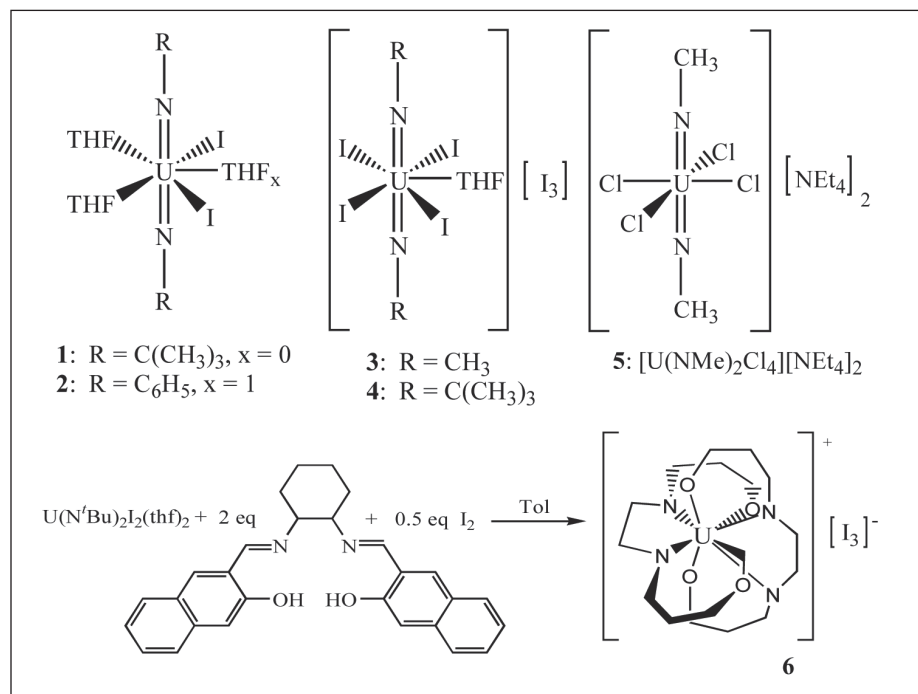
Larry Gibbons

cation (**4**) could also be synthesized from the simple addition of one equivalent elemental I_2 to the neutral bis-imido species.

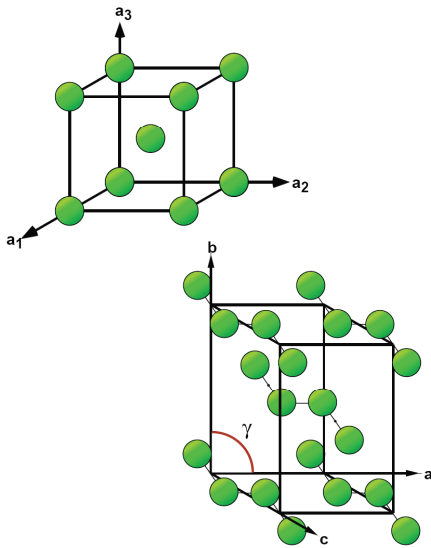
The reactivity of the methyl homologue appears to be rather constrained, being greatly limited by the sensitivity of the tri-iodide anion. However, the ability to replace the associated tetrahydrofuran molecules with other Lewis bases has been demonstrated, as has the replacement of the I_3^- ions with PF_6^- , although the final product has proved elusive in the crystalline state. The methyl cation has also been used in the synthesis of the tetrachloro-bis-methylimido dianion (**5**), the first of the methylimido species to be isolated without an associated I_3^- .

I am also interested in exploring the properties of the $RN=U=NR$ moieties themselves. To do this, large, multi-dentate organic molecules with various charges are being used to perform two important functions. First, by using a molecule with a 1- or 2- charge, the reactive iodides can be removed from the metal center. Second, by using a large, sometimes bulky organic group, the equatorial region around the metal center can be almost completely occupied, preventing it from reacting with other species that may exist in solution.

In reacting, the protonated version one of these multidentate ligands with the bis-*tert*-butylimido species, a uranium(V) cationic species was isolated without any imido ligands present (**6**). This tandem protonolysis/reduction reaction was also observed with the same uranium starting material in the presence of phenol. Not only does this reaction present a unique means of reducing the metal center through the oxidation of iodide, it also allows for an easy entry into uranium(V) chemistry, a rather elusive and unstable oxidation state for this metal center.



AMY CLARKE



Two possible uranium-niobium phases and crystal lattice structures are γ (gamma) body-centered cubic (above left) and $\alpha/\alpha'/\alpha''$ (alpha) orthorhombic, monoclinic (above right).

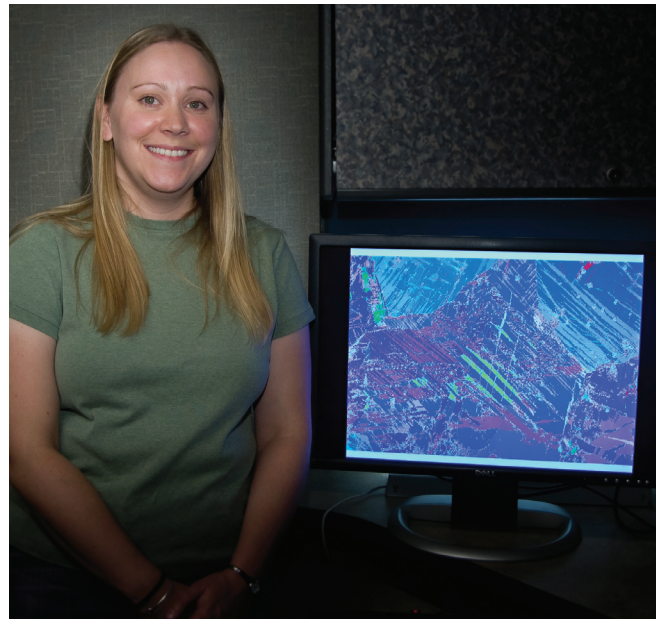
SHAPE MEMORY EFFECT DEFORMATION STRUCTURES IN A URANIUM-NIOBIUM ALLOY

Understanding the mechanical behavior and texture evolution of the uranium-niobium alloy U-14Nb (atomic percent, or at. %) is important for the development of future predictive constitutive models that describe deformation behavior of this material. In this work, detailed microstructure evolution studies are performed on deformed material, and experimental observations are compared to predictions from a single-crystal model.

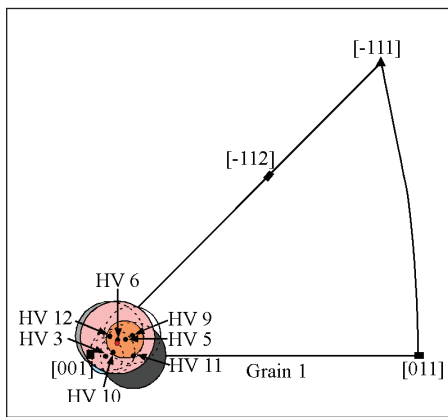
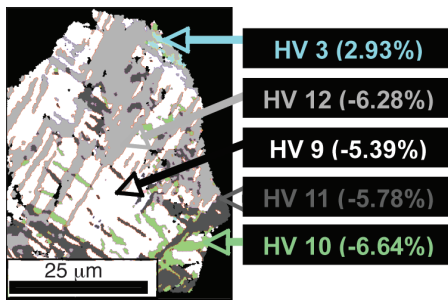
Uranium's high-temperature phase, gamma (γ)-U, has a body-centered cubic (bcc) crystal structure, while the room-temperature phase, alpha (α)-U, is orthorhombic. When U-14Nb is quenched from the γ -U phase to room temperature, it undergoes a martensite transformation to a monoclinically distorted version of α -U, referred to as α'' . Martensite transformations occur by means of lattice shear, and there are twelve possible orientations (or variants) of the monoclinic α'' in the cubic γ , all with transformation strains in different directions. These variants are all equally represented in the as-transformed structure, so there is no net macroscopic strain. They are separated by twin boundaries, across which the structure is mirrored.

When the martensite is strained, variants whose transformation strain can best accommodate the imposed strain will grow at the expense of others, via the motion of the twin boundaries, or nucleation of new twins with similar orientation relationships. There is only one way the $\alpha'' \rightarrow \gamma$ reverse transformation can proceed for each variant upon reheating, so any strain produced in this

Amy Clarke works in the Materials Science & Technology Division's Metallurgy Group (MST-6). She studied ferrous physical metallurgy at the Colorado School of Mines, where she received her doctorate in 2006. Amy began her postdoctoral appointment in May 2006. Her mentor is Robert Field of MST-6 and the Materials Design Institute, a collaborative research and educational program with the University of California, Davis. Clarke recently received the Willy Korf Award for Young Excellence for her Ph.D. work. This award is given annually to one graduate student worldwide, to recognize the contribution of their graduate research to the steel industry.



Larry Gibbons



Different colors are used to distinguish different martensite variants in this orientation imaging microscopy result (top) of an individual grain from a sample strained in compression. Using α'' and γ orientation relationships, γ orientations are shown for each martensite variant on a γ standard triangle (above). From the locus of γ orientations, a stress axis was approximated and accommodation strains for each martensite variant were calculated. Compressive strains were determined for the majority of the variants, as expected after compressive deformation. The twin boundaries between the variants corresponded to anticipated shape memory effect twinning systems. Hatt variants #5 and #6 were also observed but are not highlighted on the grain because only small fractions of these variants were present.

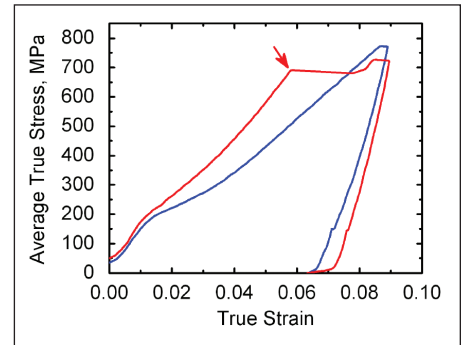
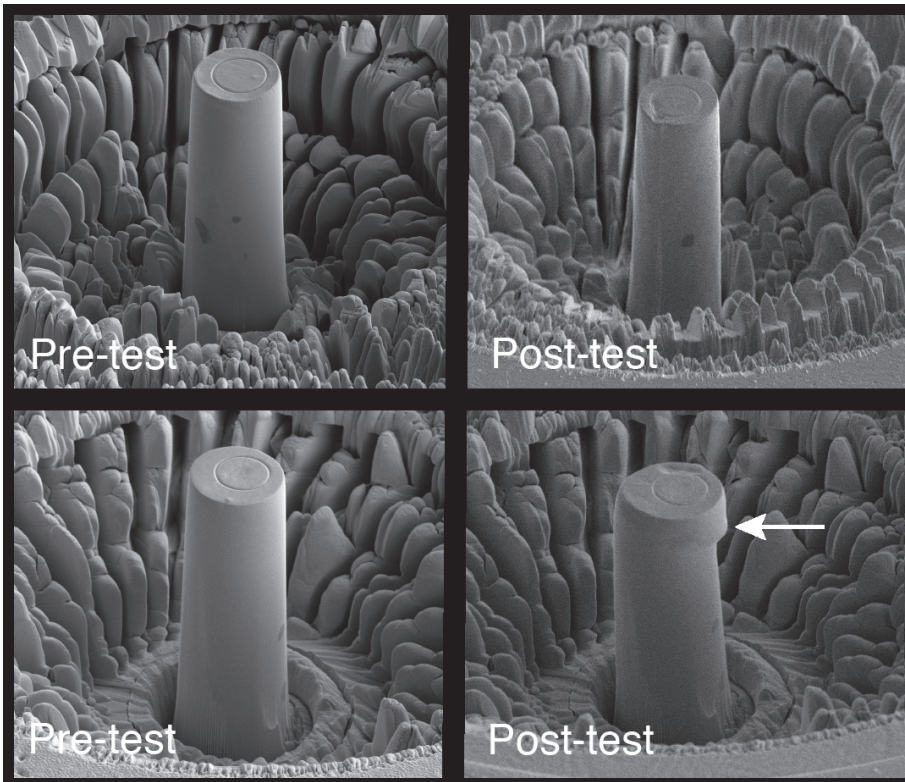
phase are also highlighted by the addition of a γ standard triangle for the most favored variant (MFV) of martensite, or the variant that best accommodates the imposed strain, anticipated to dominate in compression or tension.

The most favored variant for deformation in compression was determined to be #10 of the twelve possible martensite variants (referred to as Hatt variants, or HVs, after B.A. Hatt, reported in 1966 in the *Journal of Nuclear Materials*), while the most favored variant anticipated to dominate in tension was determined to be HV #5. The orientations shown in blue (compression example) and green (tension example) in the OIM maps and corresponding legend fall within the γ standard triangles for HV #10 and HV #5, the most favored variants for compression and tension, respectively, as predicted.

Additional analyses of the orientation imaging microscopy results were performed on individual grains from both the compression and tensile specimens. From a discrete α'' inverse pole figure (not shown), similar orientations in a grain were colored the same to distinguish the different martensite variants. Orientation relationships between the α'' martensite and the γ phase were then used to assign the appropriate number to each variant. A γ orientation for each Hatt variant was plotted on a γ standard triangle (with a circle to represent the spread in the data), and a stress axis was estimated from the locus of γ orientations for each grain analyzed. Accommodation strains for each Hatt variant were calculated from the approximated γ stress axis. Example results from a grain after compressive shape memory effect deformation are provided.

Negative strain values were calculated for nearly all of the observed Hatt variants present in the compression example. HV #10, colored green, had the highest calculated compressive strain, as expected for the most favored variant for compression. Three additional Hatt variants, colored white, light gray, and dark gray, also compose much of the grain, but have comparable strain levels to that of HV #10. Note that the γ orientation is close to [001], a symmetry position at which all four of these Hatt variants would have the same calculated accommodation strain. Thus, it is not surprising that four Hatt variants, including HV #10, constitute the majority of the grain. Tensile strains were also calculated for Hatt variants located near the grain boundaries, which likely resulted from intergranular tensile strains. The light blue color highlights one such Hatt variant, which represents a very minor constituent of the grain.

Twin boundaries between the variants were also identified with orientation imaging microscopy, and were in good agreement with predicted shape memory effect twinning systems. To study finer details of the twin structures, a focused ion beam (FIB) was used to prepare thin foils for further examination with transmission electron microscopy from specific regions of interest. Coarse twins identified with orientation imaging microscopy were confirmed with transmission electron microscopy by using select area diffraction, while finer details of the microstructure were only observable with transmission electron microscopy. Thus, orientation imaging microscopy was first used to analyze large areas, followed by subsequent transmission electron microscopy to provide



The images at left are of pre- and post-test preliminary microsamples. Initial microsample heights and diameters were ~30 microns and ~15 microns, respectively. The microsamples were fabricated from single γ grains of a polycrystalline sample using a focused ion beam. Compression testing was performed with a nano-indenter using a flat punch. The differences in stress-strain response (above) are thought to be associated with orientation dependence. Shear instability (the white arrow in the image immediately to the left) is highlighted in a post-test image for one of the preliminary samples tested, and is also reflected (the red arrow in the data plot above) in the stress-strain response for this test.

finer microstructural details. By the combination of these two complementary techniques, a predicted shape memory effect twinning system not previously observed experimentally was recently confirmed.

In this work, the single-crystal model is used to predict Hatt variants from accommodation strains and twin relationships in polycrystalline U-14Nb after shape memory effect deformation. Extension to consider post-shape memory effect (i.e., unrecoverable) deformation processes is currently under way. In addition, micro-compression samples (~15 and ~30 microns in diameter and length, respectively) from individual γ grains of a polycrystalline sample are being tested in a nano-indenter instrument with a flat punch to study the influence of γ orientation on stress-strain response and to further test the single crystal model. The stress-strain behaviors exhibited by two preliminary test samples differed, suggesting that orientation will influence the deformation response. The preliminary results are promising and support further testing with this technique.

LIAM SPENCER

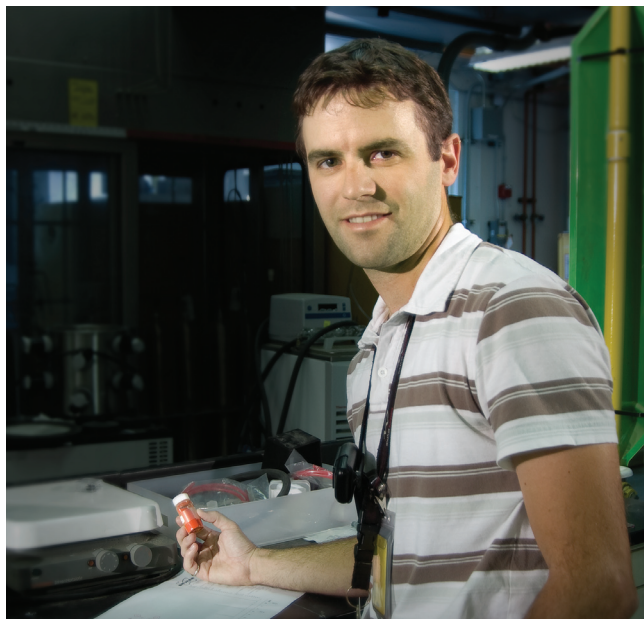
AN INVESTIGATION OF THE REACTIVITY OF A *TRANS*-BIS(IMIDO) URANIUM(VI) COMPLEX

For the past 150 years, the chemistry of uranium(VI) has been generally directed toward studies of the chemical behavior and unique bonding in the uranyl ion (UO_2^{2+}). Interest in this area is driven in part by the technological and environmental importance of uranium oxide in nuclear fuel reprocessing and waste management. Compared to the interest and vast chemistry reported for the uranyl ion, examples of the isoelectronic imido uranium(VI) analog ($-\text{U}(\text{NR})_2^{2+}$) are relatively rare.

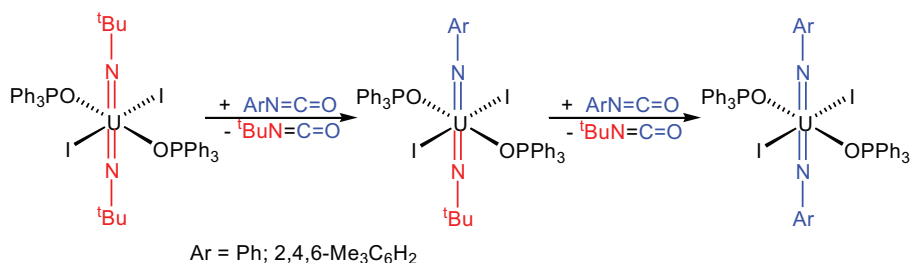
Remarkably, the synthesis and isolation of the *trans*-bis(imido) uranium(VI) complex ($\text{U}(\text{NR})_2^{2+}$) was reported in 2005 by Los Alamos researchers Trevor Hayton, James Boncella, Brian Scott, Phillip Palmer, Enrique Batista, and P. Jeffrey Hay. This discovery has allowed the opportunity to compare the valence bonding and covalency in both UO_2^{2+} and $\text{U}(\text{NR})_2^{2+}$ fragments. Density functional theory calculations show that while U–O and U–N bond interactions are similar, the bis(imido) ion possesses a more covalent nature. One question that arises from these calculations is how this reduced positive charge on the metal center influences reactivity of the $\text{U}(\text{NR})_2^{2+}$ ion.

Organic isocyanates have often been used in transition-metal chemistry to effect transformations of M=N imido functional groups. Given this precedent, the reactivity of substituted isocyanates with the $\text{U}(\text{NR})_2^{2+}$ ion was explored.

Liam Spencer works in the Materials Physics and Applications Division's Materials Chemistry Group (MPA-MC). Spencer received his doctorate from the University of British Columbia under the direction of Michael Fryzuk. His thesis project involved the study of early transition-metal N-heterocyclic carbene complexes and the activation of molecular dinitrogen by reduced transition metal complexes. Spencer began his postdoctoral appointment in October 2006. His mentor is James Boncella of MPA-MC.



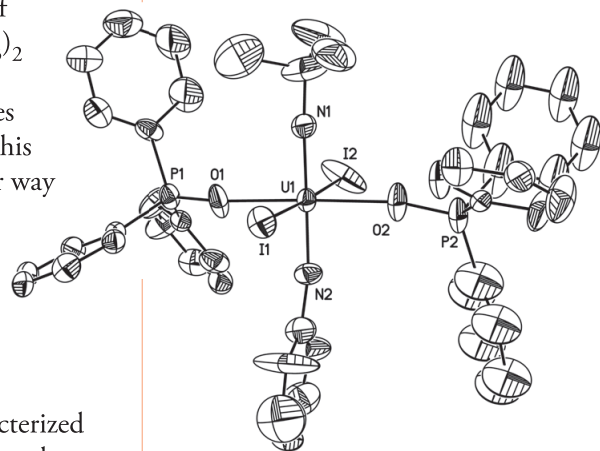
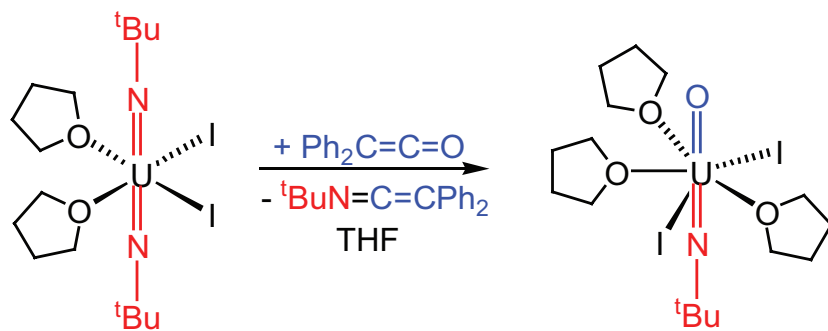
Larry Gibbons



The addition of one equivalent of aryl isocyanate (ArNCO; Ar = C₆H₅, 2,4,6-Me₃C₆H₂) to U(N^tBu)₂(I)₂(OPPh₃)₂ initiates an aryl- for alkyl-imido exchange reaction in which U(N^tBu)(NAr)(I)₂(OPPh₃)₂ is synthesized, as shown above. The solid-state molecular structure of U(N^tBu)(NAr)(I)₂(OPPh₃)₂ has been determined by X-ray crystallography and is shown in the figure at lower right.

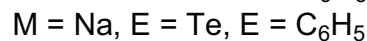
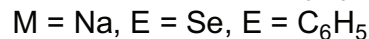
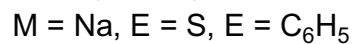
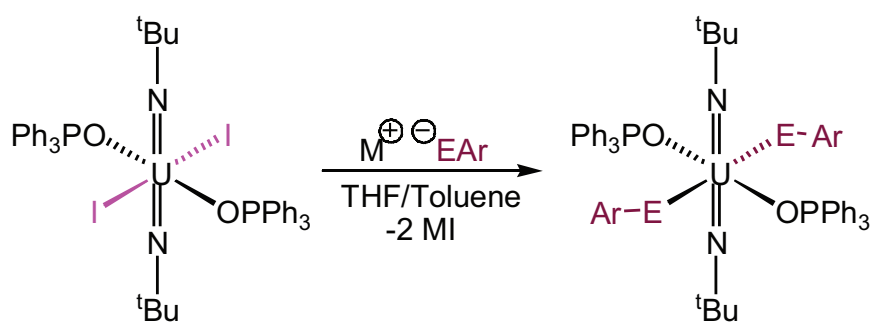
This substitution reaction can also be exploited to introduce a second aryl imido ligand as shown by the reaction between two equivalents of ArNCO and U(N^tBu)₂(I)₂(OPPh₃)₂ to generate U(NAr)₂(I)₂(OPPh₃)₂ in moderate yields. While there is precedence for this imido substitution in transition-metal chemistry, it is not clear why this reaction does not form a thermodynamic and kinetically stable U=O bond. Given this unexpected reactivity, density functional theory calculations are under way to elucidate a mechanism for this imido exchange.

The use of aryl isocyanates to accomplish exchange in this manner suggests that a similar synthetic strategy with other electrophilic cumulenes may lead to the isolation of unique uranium-heteroatom multiply bonded complexes. For example, the reaction between the U(N^tBu)₂(I)₂(THF)₂ (THF = tetrahydrofuran) and diphenylketene (Ph₂C=C=O) was examined. This reaction yields the previously characterized mixed oxo imido species U(N^tBu)(O)(I)₂(THF)₃ in reasonable yield, as shown in the following equation.

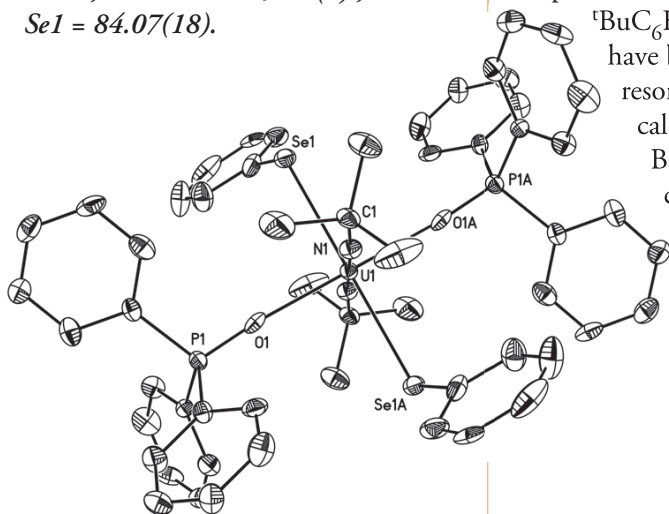


The solid-state molecular structure of [U(N^tBu)(NPh)(I)₂(OPPh₃)₂] as determined by X-ray crystallography is shown above. The following are selected bond lengths (in angstroms) and angles (in degrees): U1-N1 = 1.832(8), U1-N2 = 1.841(8), U1-O1 = 2.320(7), U1-O2 = 2.306(7), U1-I1 = 3.0623(9), U1-I2 = 3.0486(9), O1-P1 = 1.493(7), O2-P2 = 1.497(7), N1-U1-N2 = 177.4(4), N1-U1-O1 = 92.6(4), O1-U1-O2 = 178.2(3).

Investigation of hard-metal–soft-ligand interactions in the $U(NR)_2^{2+}$ ion are also of interest. To this end, the synthesis of bis(imido) uranium(VI) chalcogenate complexes has been investigated. Recent results have shown that the coordination of anionic chalcogenate donors ($-OR$, $-SR$, $-SeR$, $-TeR$) to the $U(NR)_2^{2+}$ ion can be achieved by metathesis reactions, as shown in the following equation.



The solid-state molecular structure of $[U(N^t\text{Bu})_2(\text{SePh})_2(\text{OPPh}_3)_2]$ as determined by X-ray crystallography is shown below. The following are selected bond lengths (in angstroms) and angles (in degrees): $U1-N1 = 1.861(6)$, $U1-Se1 = 2.8868(8)$, $U1-O1 = 2.360(5)$, $O1-P1 = 1.483(6)$, $N1-U1-N1A = 180.0$, $N1-U1-O1 = 90.0(2)$, $N1-U1-Se1 = 84.07(18)$.



For example, the reaction between $U(N^t\text{Bu})_2(\text{I})_2(\text{OPPh}_3)_2$ and two equivalents of NaSePh yielded the dichalcogenate complex $U(N^t\text{Bu})_2(\text{SePh})_2(\text{OPPh}_3)_2$. The solid-state molecular structure of $U(N^t\text{Bu})_2(\text{SePh})_2(\text{OPPh}_3)_2$ has been determined by X-ray crystallography and is shown in the figure at left. This methodology has been used to synthesize bis(imido) uranium(VI) chalcogenate complexes of the general formula $U(N^t\text{Bu})_2(\text{EAr})_2(\text{OPPh}_3)_2$ ($E=O$, $\text{Ar}=2\text{-}^t\text{BuC}_6\text{H}_4$; $E=S$, $\text{Ar}=C_6\text{H}_5$; $E=Se$, $\text{Ar}=C_6\text{H}_5$; $E=Te$, $\text{Ar}=C_6\text{H}_5$) which have been characterized by X-ray crystallography, nuclear magnetic resonance spectroscopy, and elemental analysis. Density functional calculations are in progress with Los Alamos researcher Enrique Batista to investigate the degree of covalency in the uranium-chalcogenate bond.

DAN SCHWARZ

STRUCTURE AND BONDING IN ACTINIDE COMPLEXES

Actinides and their binary compounds are of tremendous technological importance. They find application as fuels for nuclear power production, power supplies for deep-space exploration, and in nuclear weapons. The storage and disposal of used nuclear fuels, the disposition of facilities and wastes from nuclear weapons production sites, the transport of actinides at environmental contamination sites, and the storage lifetime of nuclear weapons pose a variety of problems that require research so that we may properly handle the material or site of concern.

The deceptively simple binary formula of the tetravalent actinide oxides, AnO_2 , hides an incredibly complex structural nature, and a tendency to form nonstoichiometric phases ($AnO_{2\pm x}$). For plutonium (Pu), it was a widely held view that compositions with oxygen/plutonium ratios higher than 2.0 were not stable. This view was challenged when the reaction of plutonium metal or oxide with water vapor was shown to produce PuO_{2+x} . This new material was examined by X-ray absorption fine structure (XAFS) spectroscopy and found to be comprised of a mixed-valent solid of Pu(IV)/Pu(V) oxidation states with short “plutonyl-like” Pu=O bonds of 1.85 angstroms (Å).

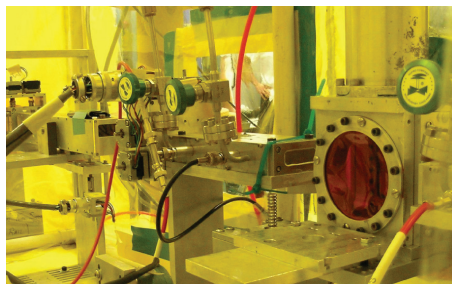
We are currently investigating similar behavior in mixed-valent uranium oxides of general formula UO_{2+x} . UO_2 and U_4O_9 ($UO_{2.25}$) have been synthesized and studied by XAFS, along with several intermediate compositions



Josh Smith

Dan Schwarz works in the Chemistry Division's Inorganic, Isotope, and Actinide Chemistry Group (C-IIAC). He received his doctorate in 2003 from the University of Illinois–Urbana-Champaign under the direction of Tom Rauchfuss. The title of his thesis was “Tetrathiomallates in Synthesis and Catalysis.” Schwarz began his Seaborg postdoctoral appointment in July 2007. His mentor is David L. Clark of the Seaborg Institute.

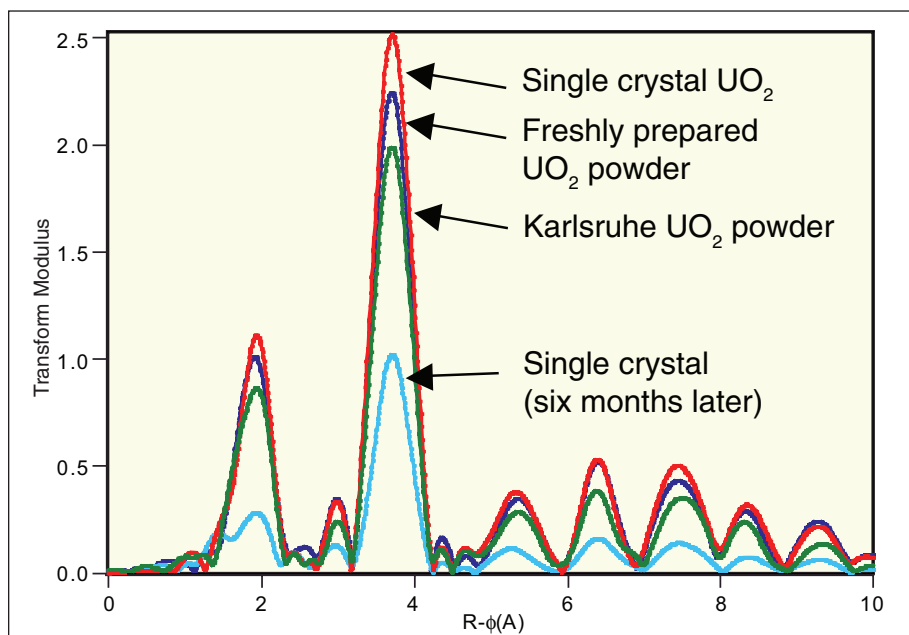
Extended X-ray absorption fine structure data comparing four samples. Higher peaks indicate greater long-range order.



A view of beamline 11-2 at the Stanford Synchrotron Radiation Laboratory where the uranium L-edge studies are performed. The yellow glow in the photo comes from a tent around the room.



The high-vacuum K-edge apparatus for X-ray absorption fine structure studies at the Stanford Synchrotron Radiation Laboratory.



of UO_{2+x} . We have found that as x increases, a new feature at 1.74 \AA , which has been assigned as $\text{U}=\text{O}$, also increases. An example of this new feature can be seen in data represented by the green line in the figure comparing different UO_2 samples.

These short contacts are not consistent with what has been previously reported using neutron diffraction and pair distribution function; however, these techniques look for long-range order, and this new short contact is a small percentage and probably highly disordered so it would not be observed by those techniques. It is only by using XAFS, which looks at local environments, that we have been able to observe the formation of this new type of bonding in a uranium oxide material. We have established XAFS capabilities at the Stanford Synchrotron Radiation Laboratory beamline 11-2 for uranium and transuranic samples.

We are also investigating the extent of covalent bonding in actinide complexes in a variety of compounds, including the isostructural UCl_6^{x-} series ($x = 1, 2, 3$). Our results challenge the dogma of actinide chemistry that $5f$ electrons don't contribute to the formation of covalent bonds. In fact, our data show that UCl_6^{2-} has about half the covalency found in transition metals with contributions from both the $6d$ and $5f$ orbitals. We plan to extend our analysis beyond chlorine (Cl) edges to include oxygen (O) and nitrogen (N) edges, which would require ultra-high vacuum and a special chamber. Improving our understanding of the extent of covalent bonding can aid in ligand design for fuel separation and reprocessing.

Actinide Research Quarterly
is published by Los Alamos
National Laboratory

Actinide Research Quarterly

is a publication of the
Stockpile Manufacturing and
Support (SMS) Directorate.

The directors of the Seaborg Institute for
Transactinium Science serve as the magazine's
scientific advisors. *ARQ* highlights progress
in actinide science in such areas as process
chemistry, metallurgy, surface and separation
sciences, atomic and molecular sciences,
actinide ceramics and nuclear fuels,
characterization, spectroscopy, analysis,
and manufacturing technologies.

Address correspondence to
Actinide Research Quarterly
c/o Meredith Coonley
Mail Stop G756
Los Alamos National Laboratory
Los Alamos, NM 87545

ARQ can be read online at www.lanl.gov/arq

If you have questions, comments, suggestions,
or contributions, please contact the
ARQ staff at arq@lanl.gov.

Phone (505) 667-0392
Fax (505) 665-7895

ARQ Staff

SMS Associate Director

Carl Beard, Acting

*Scientific Advisors,
Seaborg Institute*

David L. Clark

Gordon D. Jarvinen

Contributing Scientific Advisor

Albert Migliori, Seaborg Institute and MPA-NHMFL

Editor

Meredith S. Coonley, IRM-CAS

Designer

Kelly L. Parker, IRM-CAS

Contributing Editor

Ed Lorusso, CT-PPI

Contributing Photographers

Larry Gibbons, IRM-RMMSO

Josh Smith, C-DO

Printing Coordinator

Lupe Archuleta, IRM-RMMSO



Los Alamos National Laboratory, an affirmative action/equal opportunity employer, is operated by Los Alamos National Security, LLC, for the National Nuclear Security Administration of the U.S. Department of Energy under contract DE-AC52-06NA25396.

This publication was prepared as an account of work sponsored by an agency of the U.S. Government. Neither Los Alamos National Security, LLC, the U.S. Government nor any agency thereof, nor any of their employees make any warranty, express or implied, or assume any legal liability or responsibility for the accuracy, completeness, or usefulness of any information, apparatus, product, or process disclosed, or represent that its use would not infringe privately owned rights. Reference herein to any specific commercial product, process, or service by trade name, trademark, manufacturer, or otherwise does not necessarily constitute or imply its endorsement, recommendation, or favoring by Los Alamos National Security, LLC, the U.S. Government, or any agency thereof. The views and opinions of authors expressed herein do not necessarily state or reflect those of Los Alamos National Security, LLC, the U.S. Government, or any agency thereof. Los Alamos National Laboratory strongly supports academic freedom and a researcher's right to publish; as an institution, however, the Laboratory does not endorse the viewpoint of a publication or guarantee its technical correctness.

LALP-07-040



